المجلة الإلكترونية الشاملة متعددة التخصصات
العدد الخامس والستين شهر (10) 2023

Surface modification of MXene Nanosheet/Polymer for biomedical applications.

Mariam Ghazi Awad Alrasheedi
PhD student in Medical Physics, Faculty of science king AbdulAziz University.
Jeddah,Saudi Arabia.
Nuclear Physics lecturer,Department of Physics,College of Science and Arts ,Qassim University.
Qassim,Saudi Arabia.

Dr.Maged Faihan Alotaibi
Faculty of science king AbdulAziz University.
Jeddah,Saudi Arabia.

Prof. Nihal Saad Elbialy
Faculty of science king AbdulAziz University.
Jeddah,Saudi Arabia .

Abstract

Here we present a facile method to produce a modified Ti_3C_2Tx from Max Phase Ti_3AlC_2 powder by etching. This process helps in controlling the characteristics and structure of MXene (MX). Then, MX was loaded with curcumin (cur) and surface modified with polyethylene glycol (PEG) forming (PEG-MXNS@cur). The physicochemical characterization of MX and PEG-MXNS@cur were investigated using several techniques. The results showed the successful preparation of both MX and PEG-MXNS@cur. Encapsulation efficiency of curcumin was 99%. The drug release profile showed a cumulative release rate of 53% at 24 h and 73.5% at 96 h at pH 5 and at pH 7.4, curcumin showed a release of 1.4 % at 24 h and 2.25% at 96 h. Using DPPH assay, MX and PEG-MXNS@cur exhibited high antioxidant activity. Moreover, both MX and PEG-MXNS@cur showed a cytotoxic effect on MCF7 and HepG2 cell lines, while PEG-MXNS@cur showed IC_{50} values of 90.19 and 98.95 µg/ml for MCF7 and HepG2 cell lines,

respectively. These findings suggest that PEG-MXNS@cur has the potential to be used as a therapeutic agent to treat cancer with no or little side effects. This surface modification method is also simple and easy to adopt in MXene-based research.

Keywords: Mxene, Mxene loaded curcumin, Physicochemical characterization, Cytotoxicity, Antioxidant activity.

1. Introduction

Currently, cancer is regarded as one of the world's major causes of death. Annually, more than 10 million individuals receive a diagnosis of the illness, and more than 760 million people pass away from it [1]. In terms of incidence among women worldwide, breast cancer alone is reported as the fifth leading cause of death [2].

The most conventional strategy used for cancer therapy is chemotherapy. Chemotherapy is typically administered at some point during the course of cancer treatment. Even though chemotherapy plays a crucial role in the treatment of cancer patients, it has serious limitations in terms of therapeutic efficacy, including dose restrictions, unwanted severe side effects, and drug resistance. Extensive research on the cellular, molecular, and genetic levels has offered a promising window into the development of alternate strategies such as nanotechnology, for battling cancer with little side effects. Nanotechnology-based cancer therapy management is one of the urgent needs for innovative, potent, and secure anticancer drugs [3–4].

MXenes are 2D carbide and nitride nanomaterials that were found in 2011. They have a high melting point, good biocompatibility, and strong metallic electrical conductivity [5–6]. Due to the abundance of surface functional groups, MXenes can be altered with a variety of substances to improve their characteristics and broaden their applicability. MXenes have more functional groups on their surface than other 2D materials, which makes modification easier. MXenes are suited for use in biomedical applications because they have entire metal atomic layers, an adjustable composition, and

hydrophilicity. Additionally, MXenes may be preferable due to their efficient scale-up synthesis [6].

Despite having superior permeability and retention properties and the potential to aggregate at the tumour site, nanosized Ti_3C_2 the first MXene for drug delivery vehicles needs to be surface modified since it restacks under physiological circumstances. The modified MXenes have the ability to carry and release medicines with precision [7]. Polyethylene glycol (PEG)-treated MXene has also demonstrated encouraging results as anticancer agents and is far less harmful to normal cells [8].

The primary yellow pigment obtained from turmeric (Curcuma longa) is known as curcumin and is frequently utilised as a food flavouring agent [9]. Due to its medicinal properties in Indian and Chinese medicine, curcumin has been extensively researched for its anti-inflammatory, anti-angiogenic, antioxidant, wound-healing, and anti-cancer effects [10]. Curcumin also exhibits anti-proliferative and anti-carcinogenic characteristics in a range of cell lines and animals, according to extensive studies [11]. Additionally, recent research has demonstrated that curcumin can effectively cause apoptosis whether used alone or in conjunction with other anticancer drugs [10].

The present study aimed to surface modify MXene nanosheet with PEG (PEG-MXNS) and combine the medicinal plant curcumin for better biosafety profile. Curcumin is encapsulated with PEG-MXNS (PEG-MXNS@Cur) to enhance its bioavailability and its cancer therapeutic efficacy. The current work assessed the therapeutic efficacy of PEG-MXNS@Cur in comparison with free MXNS against hepatocellular carcinoma (HepG2) and breast cancer cell lines (MCF7) by measuring cytotoxicity using MTT (3-(4.5-dimrthylthiazol-2-yl)-2,5-diphenyltetrazolium bromide) assay, encapsulation efficiency, total antioxidant activity using DPPH scavenging assay, and drug release profile.

2. Materials and Methods

2.1 Materials

The basic ingredients used in the synthesis of MXene were: MAX Phase powder of Ti_3AlC_2 from (NANO SHEL. India), hydrofluoric acid from (HF, Panreac AppliChem IT Reagents) and deionized water. The pH meter was used for adjusting pH values in the experiment of Ph obtained from Sigma-Aldrich. All aqueous solutions were prepared using deionized water. Dimethyl sulfoxide (DMSO) (Merk, Darmstadt, Germany). Hepatic carcinoma (HepG2) and breast cancer (MCF7) were the two human cancer cell lines utilized in the present investigation. It has been supplied by the American Type Cell Culture Collection (ATCC, Manassas, USA) and were kept at VACSERA, Giza, Egypt. Sigma Aldrich (USA) supplied the chemicals, namely 2,2-diphenyl-1-picrylhydrazyl (DPPH) and butylated hydroxyl toluene (BHT).

2.2 Methods

2.2.1 Fabrication of drug loaded and unloaded MXene nanoparticles.

2.2.1.1 Fabrication of MXene nanosheet (MXNS)

Hydrofluoric acid (60 ml) was added to 3 g Ti_3AlC_2 powder stirred for 24 h at ambient temperature. Ti_3AlC_2 powder will be etched by hydrofluoric acid. 5 ml of distilled water was used to wash the reaction product. The washing was repeated several times to get rid of Al and to raise the mixture's pH above 6. Centrifugation was then used to separate the colloidal solution (Al free) Ti_3C_2Tx from the supernatant by rotating it for 30 minutes at 4000 rpm. The resulting solution of MXene was dehydrating in an oven at 80 °C for a holding time of 12 h. Finally, Mxene powder was collected for further use.

2.2.1.2 Fabrication of Polyethylene glycol -Mxene- curcumin nanosheet (PEG-MXNS@cur)

In 25 ml of 0.1% w/v DMSO, 100 mg of Mxene was added and dissolved using magnetic stirrer. Then, 30 mg of curcumin was dissolved in 100 µl DMSO (0.1% w/v) then the volume was completed to 15 ml deionized water at 50˚C. Curcumin solution was dropwise poured to Mxene solution under magnetic stirrer (DIAHAN Scientific, Korea) for 6 h. The mixture was then

incubated overnight at 37 °C in a water bath shaker for improved drug loading. Centrifuging curcumin loaded with MXxene for 10 minutes at 6000 rpm separated the loaded from the unloaded curcumin... Finally, the precipitated Mxene -curcumin nanosheets were resuspended in deionized water and the formed solution was kept for further use. At the end, add 50 microliter PEG-THIOL to the resuspend nanosheets, vortex and keep it in the fridge.

2.2.2 Physicochemical Characterization

2.2.2.1 FTIR spectroscopy:

The Perkin Elmer Spectrum 100 FT-IR analyzer was used to measure FTIR spectra for MX and PEG-MX@cur. Measurements were performed between the wavenumbers of 400 and 4000 cm^{-1}. The obtained results were recorded and plotted. In FTIR measurements, a drop from liquid samples was placed between two KBr plates to get a thin layer of the sample. These plates are then placed inside the machine and the test is started. Once the test started, IR light from the source passed through the interferometer to the specimen. The absorbance of the IR light by the aggregate takes place wherever IR beam frequency matches with that of the sample and the spectrum is recorded.

2.2.2.2 UV-VIS spectroscopy

Shimadzu (Japan) UV-Vis-NIR 3600 spectrophotometer was used for optical spectroscopic analysis. The optical properties of the samples were measured over wavelength range 200 to 800 nm. The obtained results were recorded and plotted.

2.2.2.3 Dynamic Light Scattering (DLS) and Zeta Potential

Dynamic Light Scattering (DLS) instruments were utilized to study the hydrodynamic size distribution and polydispersity index of MX and PEG-MX@cur (Zeta sizer Nano ZN, Malvern Paralytical Ltd., UK). The specimens were measured in triplicate. A zeta sizer was also used to measure zeta potential values for MX and PEG-MX@cur. In a disposable capillary cell, a sample is inserted to measure zeta potential value.

2.2.2.4. Scanning electron microscope (SEM)

The external features and composition of MX was visualized using JSM-7600F FE-SEM from JEOL, JAPAN. Energy-dispersive X-ray spectroscopy (EDX) mode has been helpful when used in conjunction with the SEM to precisely detect the elemental composition.

2.2.2.5. Transmission electron microscope (TEM)

Morphology and structure of MX was recorded using a high-resolution transmission electron microscope (HRTEM; Japan-made JEOL Model JEM 2100F working at 200 kV).

2.2.3 Biomedical applications

2.2.3.1 Cytotoxic study by MTT assay

The MTT (3-(4.5-dimrthylthiazol-2-yl)-2,5-diphenyltetrazolium bromide) assay was used to evaluate the cytotoxic activity of the test compounds in accordance with the published technique [12-13]. The yellow tetrazolium bromide (MTT) in this colorimetric assay is converted into a purple formazan derivative by the mitochondrial succinate dehydrogenase found in living cells. Cells were plated in 96-well plates with 10% fetal bovine serum in DMEM for 24 hours. Then, DMSO was used as a vehicle for treating cells, testing chemicals, and reference medications for 48 hours. The cells were subsequently treated for 2 hours with 200 µl of DMEM that contained 0.5 mg/ml of MTT. After removing the supernatant, 200 µl of DMSO were used to dissolve the formazan precipitate. The absorbance at 570 nm was then measured using a microplate reader. The relationship between cell viability % and drug concentration was plotted [14-18]. The proportion of relative cell viability was calculated as (A570 of treated samples/A570 of untreated samples) x100. The concentrations of Mxene and PEG-MX@cur nanosheets that inhibit 50% of cell growth were used to obtain the IC_{50} values.

2.2.3.2 Antioxidant viability

The scavenging activities of Mxene, PEG-MX@cur and Curcumin free radicals were estimated using DPPH radical method [19]. Various proportions (50, 100, 200, 400, 600, 800, and 1000 µg/ml) of the Mxene and PEG-MX@cur nanosheets and (12.5, 25, 50, 100, 150, 200 and 250 µg/ml) of the preparation of curcumin used deionized water. Afterwards, 0.1 ml of Mxene, PEG-MX@cur, and Curcumin were added to 1 ml of freshly made ethanol-based 0.1 mM DPPH solution. Before the absorbance at 515 nm was measured with a UV spectrophotometer, the mixtures were agitated and let to sit for 30 minutes at room temperature. The control samples were intended to be samples devoid of nanosheets. The control samples were chosen to be the ones free of nanosheets. The positive control used for the duration of the activity was butylated hydroxyl toluene (BHT), which was synthesized in the same concentration as the nanosheets. Due to the free radical scavenging activity, which was identified as follows, the DPPH absorbance was decreased:

$$\text{DPPH radical Scavenging activity} = \frac{\text{Abs C} - \text{Abs S}}{Abs\ C} \times 100\ \%.$$

where Abs S is the absorbance of the sample or the standard, and Abs C is the absorbance of the control.

2.2.3.2.1 IC_{50} Statistical analysis for the antioxidant activity

Using a linear regression approach, the scavenging rate (%) versus the amount of Mxene nanosheets accessible was used to calculate the IC_{50} values. To calculate IC_{50} from antioxidant activities data by using Excel regression equation:

$y = B\ x + A$

Here, x is an independent variable, whereas y is a dependent variable. The coefficients are B and A.

$IC_{50} = (50 - b)/a$. While A and B are regression coefficients.

2.2.3.3 Drug release profile test

The drug release study of the prepared PEG-MXNS@cur nanosheets was conducted using dialysis bag method. Release studies were performed for samples incubated at different pH (5.5, 7.4) simulated the tumor micro-environment and normal cells, respectively [20]. Because curcumin is poorly soluble in water, release media containing 0.5% T-80 in phosphate buffered saline (pH 7.4, 5.5) was utilized. 2 ml of PEG-MXNS@cur with 0.4 mg drug was loaded into standard cellulose dialysis tubing with MWCO of 12-14 kDa. In a water bath that was shaking at 37 °C, 40 ml of release medium was added to the dialysis tube. At 1, 2, 3, 4, 5, 6, 24, 48, 72, and 96 hr. 2 ml of the dissolution medium was taken, and the fluorescence emission was recorded at excitation λ = 420 and emission λ =530. Based on a calibration curve, the total amount of released curcumin was determined, and the cumulative percentage release was calculated [21].

$$\text{Percentage Released} = \frac{\text{Mass of released curcumin}}{\text{Total Mass of curcumin}} \times 100\ \%$$

2.2.3.4 Encapsulation efficiency measurements

PEG-MXNS@Cur was centrifuged at 6000 rpm for 10 min to separate the non-encapsulated drug then, the supernatant was completed to 40 ml 0.1% DMSO in water and the sample was measured in triplicate. Stock solution of curcumin in 0.1% DMSO in water with a concentration of 10 µg/ml was prepared and diluted to make a calibration curve. Finally, the samples were measured using UV-spectrophotometer (JANEWAY 6305 spectrophotometer) at wavelength = 425 nm. The encapsulation efficiency was measured using this following equation:

$$Encapsulation\ efficiency \quad \frac{intial\ amount\ of\ Cur - unloaded\ Cur\ in\ superntant}{intial\ amount\ of\ Cur}\ x\ 100$$

3. Results and Discussion

3.1 FTIR spectroscopy

Fourier transform infrared (FTIR) spectroscopy is used for examining the physical characteristics of solids, liquids, and gases. The functional groups of both MXNS and PEG-MXNS@Cur were measured using FTIR spectroscopy, Fig. 1(a) and (b).

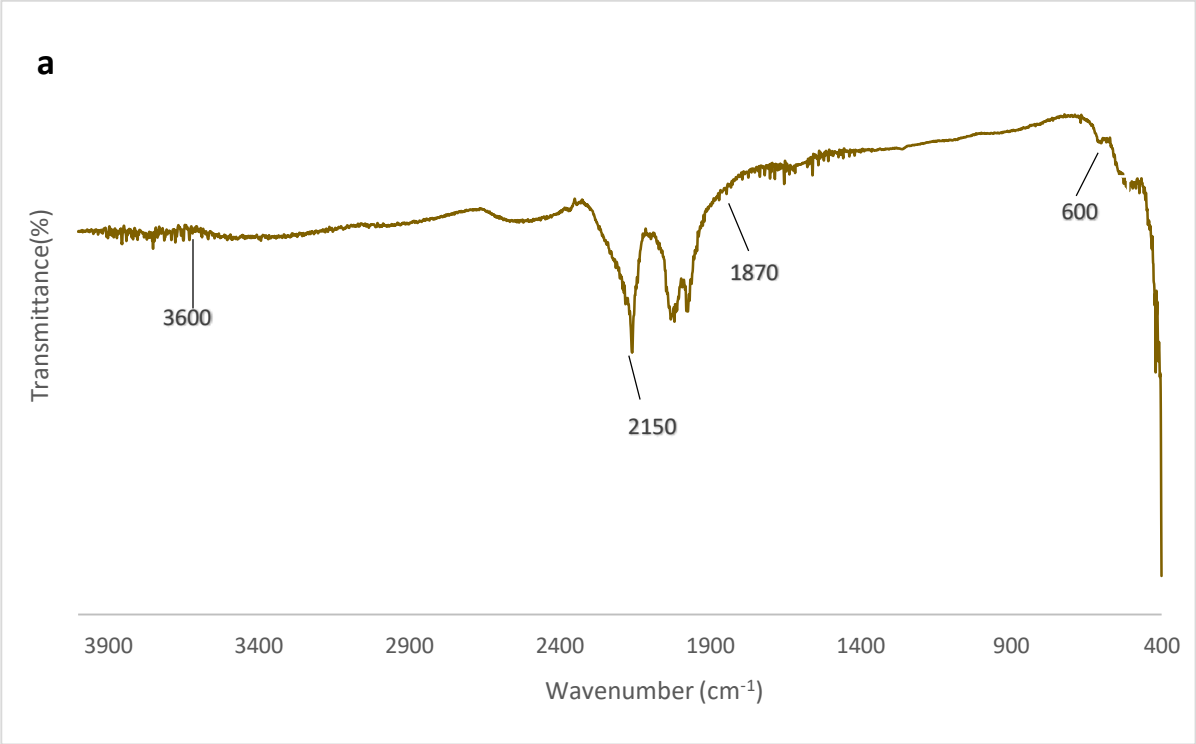

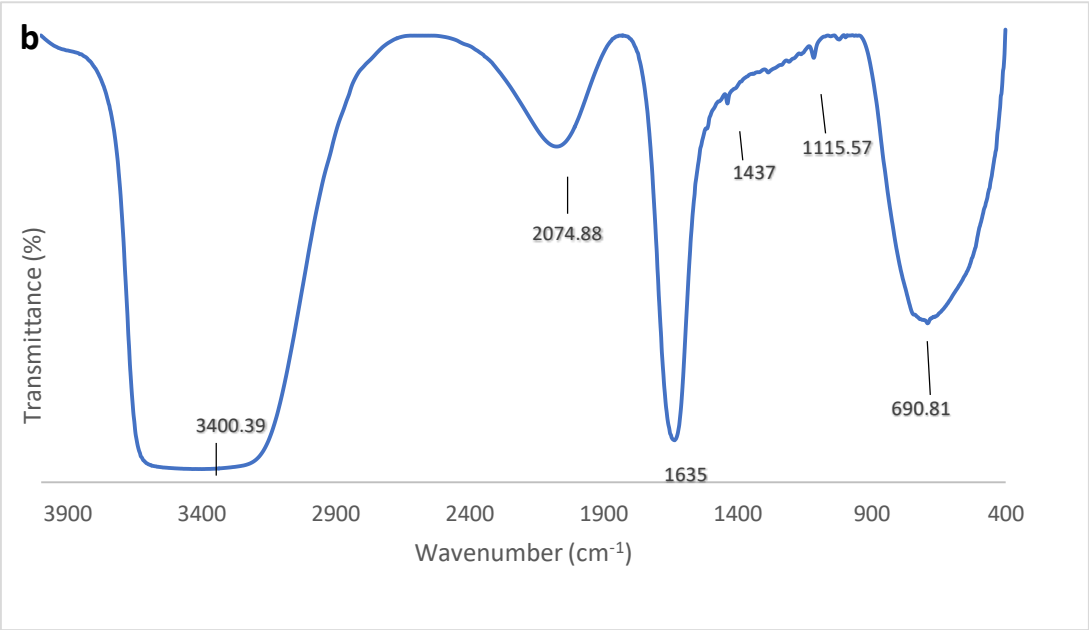

Fig. 1: FTIR spectra for (a) MXNS and (b) PEG-MXNS@Cur.

In Fig. 1a, MXNS spectrum exhibited peaks between 1800 cm^{-1} to 2200 cm^{-1} corresponding to the C=O group. In addition to the presence of some peaks that could be observed between 3600 to 3900 cm^{-1}, this vibrational pattern is due to the O-H functional group [22]. Ti-O functional group is characterized by the peak at 600 cm^{-1} [23].

In Fig. 1b, PEG-MXNS@Cur spectrum showed peaks at 3400 cm^{-1} and 2074 cm^{-1} that corresponds to the OH group, -C=O group, O-H group at around 1635 cm^{-1}, -OH group at around 1437 cm^{-1}, C-F group at 1115 cm^{-1} and finally 690 cm^{-1} corresponds to Ti-O respectively [23]. In addition, it can be inferred that peaks in the range of 1600 cm^{-1} and 2100 cm^{-1} are visible in MXene-Curcumin spectrum, which agrees with the existence of the C=O group. A vibrational broad pattern is also seen at around 3400 cm^{-1}, which is caused by the absence of atmospheric moisture and correlates to the O-H functional set.

The peak found at 690 cm^{-1} is consistent to the Ti-O functional group, and matches well with the existing literature [22-23]

3.2 UV-VIS spectroscopy

MXNS and PEG-MXNS@Cur's optical response were measured using UV-VIS spectroscopy. In Fig. 2(a), MXNS spectrum showed absorption peaks at 260 nm and 700 nm because Ti_3C_2 is black in color and has a distinct absorption edge [24]. The UV-Vis absorption band's broadness is closely connected to the previously described optical properties of Mxenes; the localized surface plasma resonance (LSPR) phenomenon might be responsible for such unique attributes. Similarly, Fig. 2 (b). showed PEG-MXNS@Cur absorption spectrum, although the color of the solution is blackish green and has a distinct absorption edge, nevertheless a strong optical peak can be detected over the wavelength range between 250 and 800 nm, as shown in Fig.2b. This UV-Vis absorption band's broadness is closely connected to the previously described optical properties of Mxenes and Curcumin [25-27]. The PEG-MXNS@Cur exhibits a significant absorbance in between 265-300 nm region. A broad spectrum from 370- 520 nm is also observed with an associated increase in the absorption intensity compared to 435 nm for pure curcumin in DMSO [28]. Consequently, the UV-Vis bands show that the interaction combination between Mxene and curcumin was successfully formed.

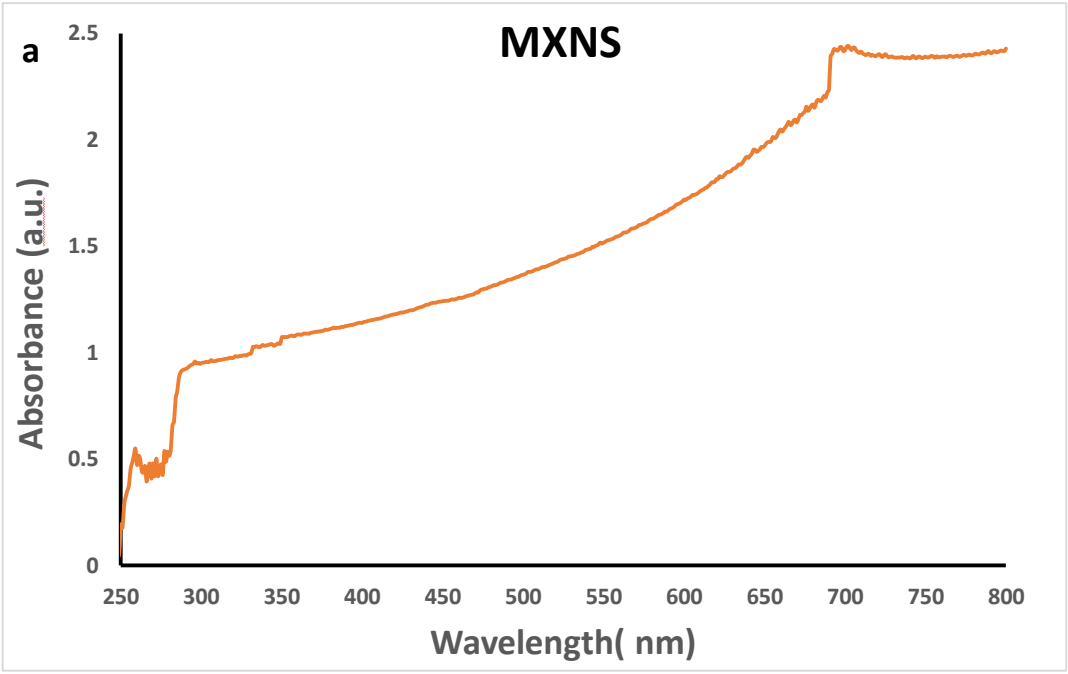

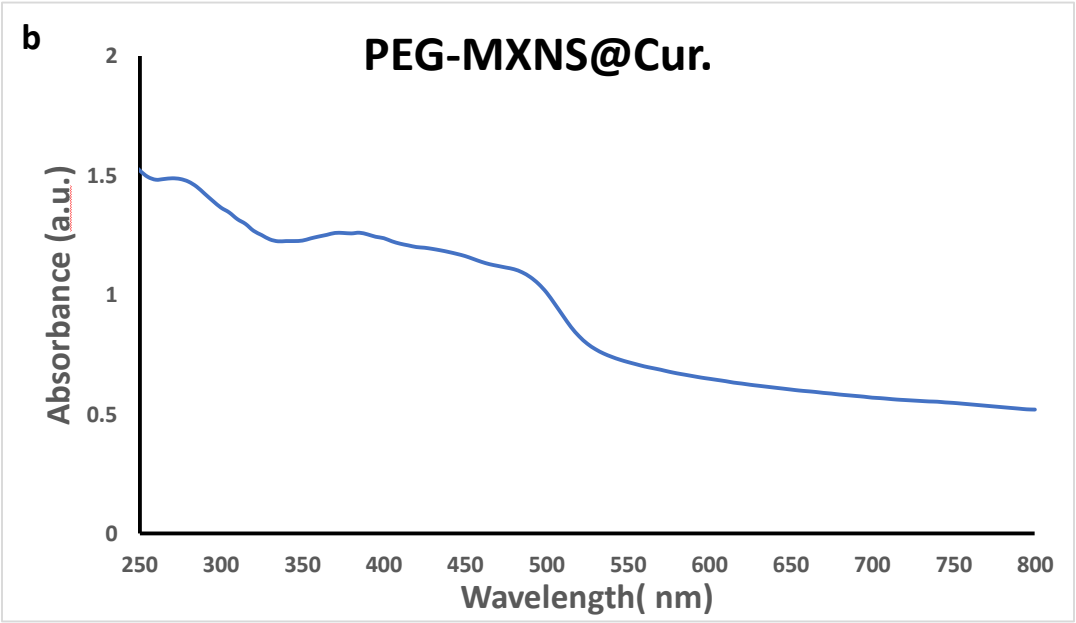

Fig. 2: UV-Vis Spectroscopy for (a) MXNS and (b) PEG-MXNS@Cur.

3.3 Zeta Potential Measurements

To evaluate MXNS and PEG-MXNS@Cur s' zeta potential, zeta sizer instrument has been used. The measured zeta potential values of MXNSs were -24 ± 3.85 mV, and PEG-MXNS@Cur was -21.3±3.6 mV. The surface charge of MXNSs was negative which agreed with a previous study [30], but the measured zeta potential in the present study was better indicating the stability of the synthesized MXene. After curcumin loading, the negativity decreased to -21±3.6 mV [31].

a

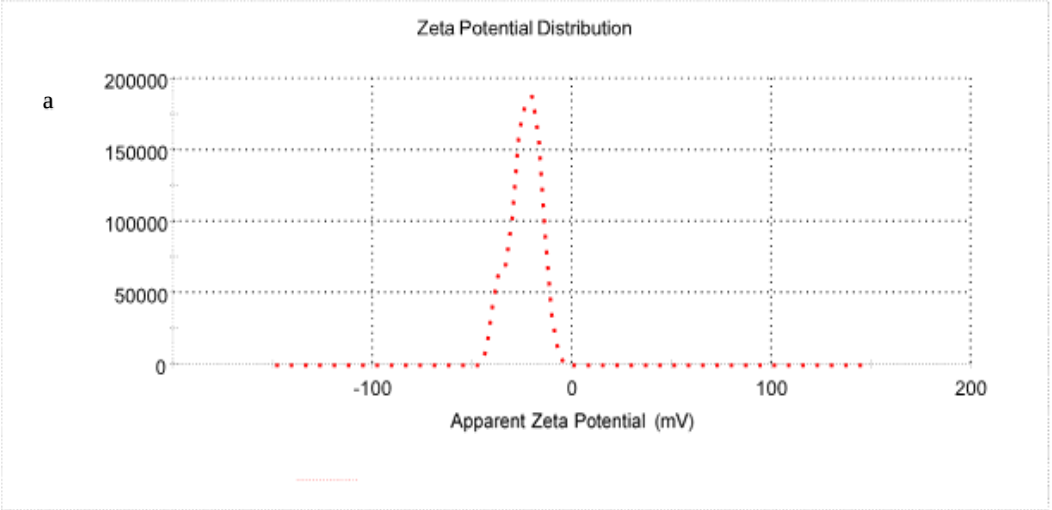

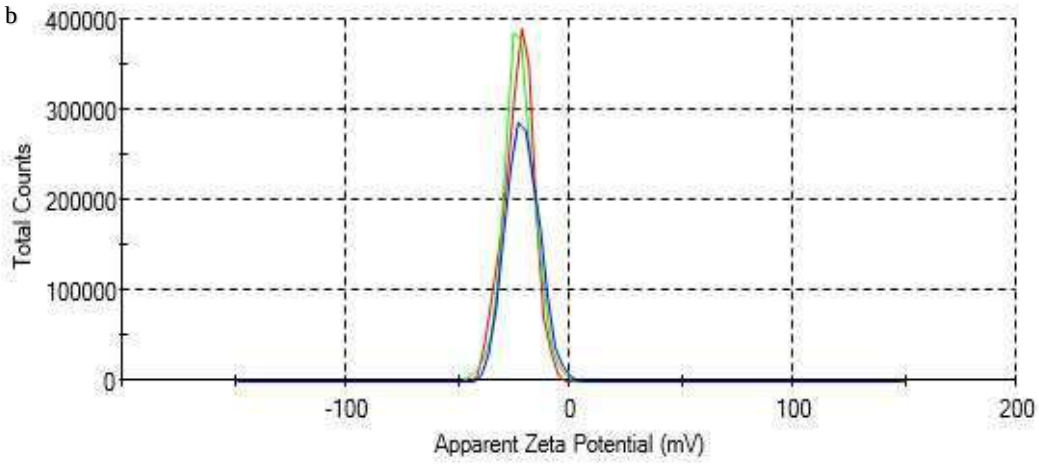

Fig. 4: Zeta Potential (a) MX (b) PEG-MX@cur.

3.4 Scanning electron microscope (SEM)

Figure 5 shows that MXene was successfully exfoliated from the MAX phase once it has been etched with hydrofluoric acid (HF) solution. Since Al forms a weak metallic bond with Ti and C, Al is selectively removed during continuous HF etching of the MAX phase. The resulting MXene's have multiple stacked 2-dimensional Ti and C layers.

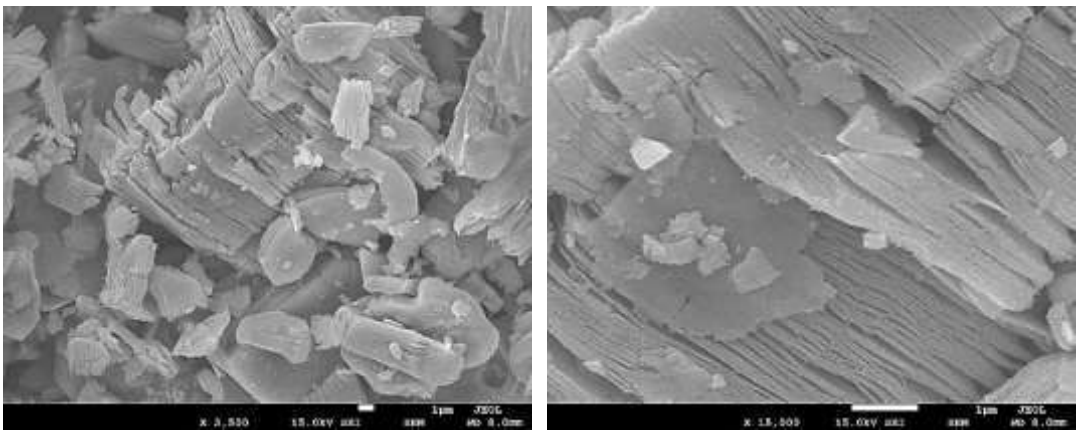

Fig. 5: SEM images at different magnifications.

Additionally, Mxene's composition was detected via energy dispersive spectroscopy (EDX) to be Ti, C, O, and F with minor quantities of metallic aluminum as shown in the figure 6.

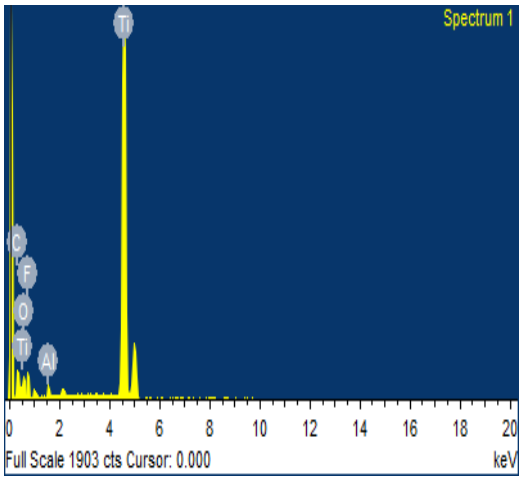

Fig. 6: EDX of the MXene.

And the values of the content of the elements found in the MXene are tabulated in table 1. The findings in fig. 6 indicate that the Al monolayers might be substituted by O_2 i.e., (OH) and/or fluorine. To eliminate OH and F, MXene powders can be further treated by annealing [32-36].

Table 1: Content of elements in MXene:

S. No	Element	Weight (%)	Atomic (%)
1	Titanium	70.00	44.08
2	Carbon	6.38	16.02
3	Oxygen	9.23	17.39
4	Fluorine	13.63	21.65
5	Aluminum	0.77	0.86

3.5 Transmission electron microscope (TEM)

The images shown in below fig. 7, demonstrate some of the acquired TEM images. As expected, particles would agglomerate as the solvent evaporates before characterization. Some of these

nanoparticles are depicted in higher magnification images in Figs. 7 (a &b). The corresponding high-resolution TEM image of MXene demonstrates that the nanoparticles are between 15 and 25 nm in size [37-39].

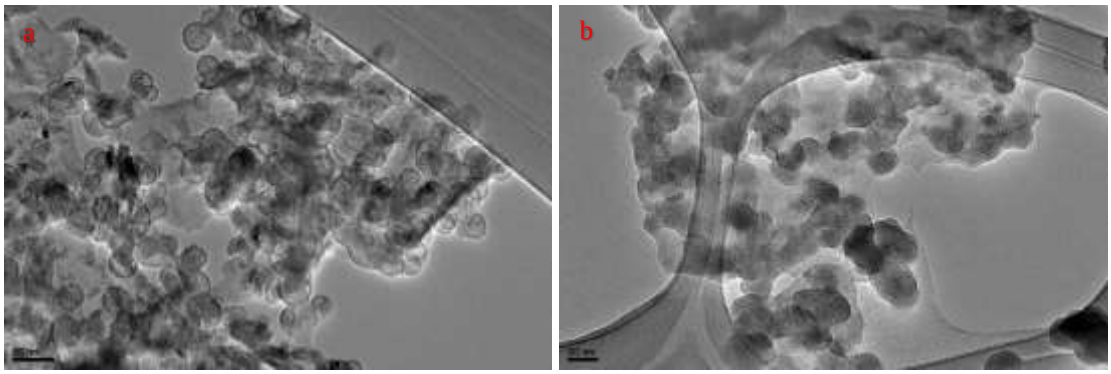

Fig. 7: TEM images of MXNS.

3.6 In vitro anticancer activity

3.6.1 Cytotoxicity measurements against HepG2

The cytotoxicity of MXNS and PEG-MXNS@Cur were determined using MTT assay. HepG2 cell line exposed to 0.98, 1.95, 3.91, 7.81, 15.63, 31.25, 62.5, 125, 250, 500, 1000 and 2000 µg/ml for the Mxene and to 0.98, 1.95, 3.91, 7.81, 15.63, 31.25, 62.5, 125 and 250 µg/ml for the PEG-MXNS@Cur at incubation time of 48 h. Cell viability tests revealed that Mxene suppressed the growth HepG2 cell in a dose-dependent manner (Figure 8(a)). However, Mxene caused growth inhibition of 13.26 % at a very high concentration of 2000 µg/ml which indicates that Mxene has a poor anticancer ability with lower concentrations. Furthermore, the Mxene IC_{50} value was 1546 µg/ml which correlates with the poor inhibition activity for the Mxene at low concentrations (figure 8 (c)). On the other hand, the cytotoxicity of PEG-MXNS@Cur showed a promising inhibition activity with lower concentrations than Mxene alone. Figure 8 (b) presents the values for PEG-MXNS@Cur nanosheetes at maximum concentration of 250 µg/ml with a viability percentage of 12.89

% which is much lower compared to Mxene alone. These findings suggest that the addition of curcumin to Mxene significantly increased its anticancer properties; this is because the polyphenol present in curcumin has anticancer properties [40]. Accordingly, the IC_{50} results of the Mxene Curcumin was 98.95 µg/ml (figure 8 (c)) which is very much lower than Mxene alone [41].

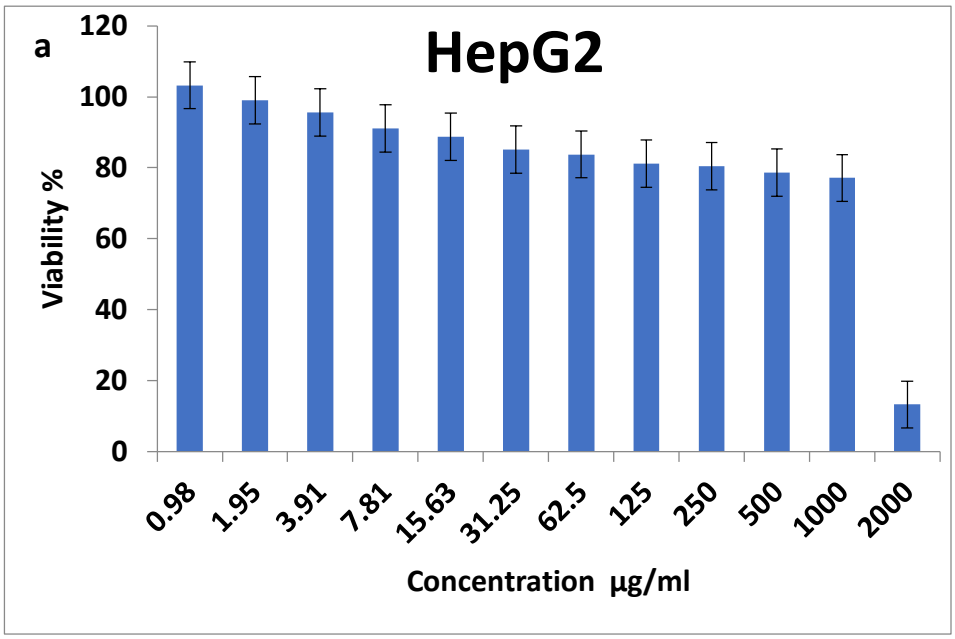

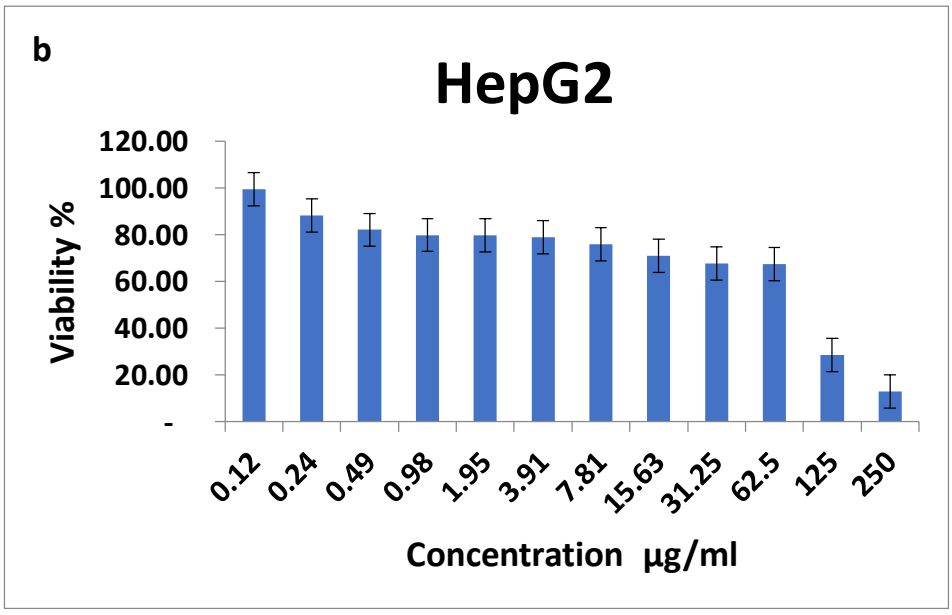

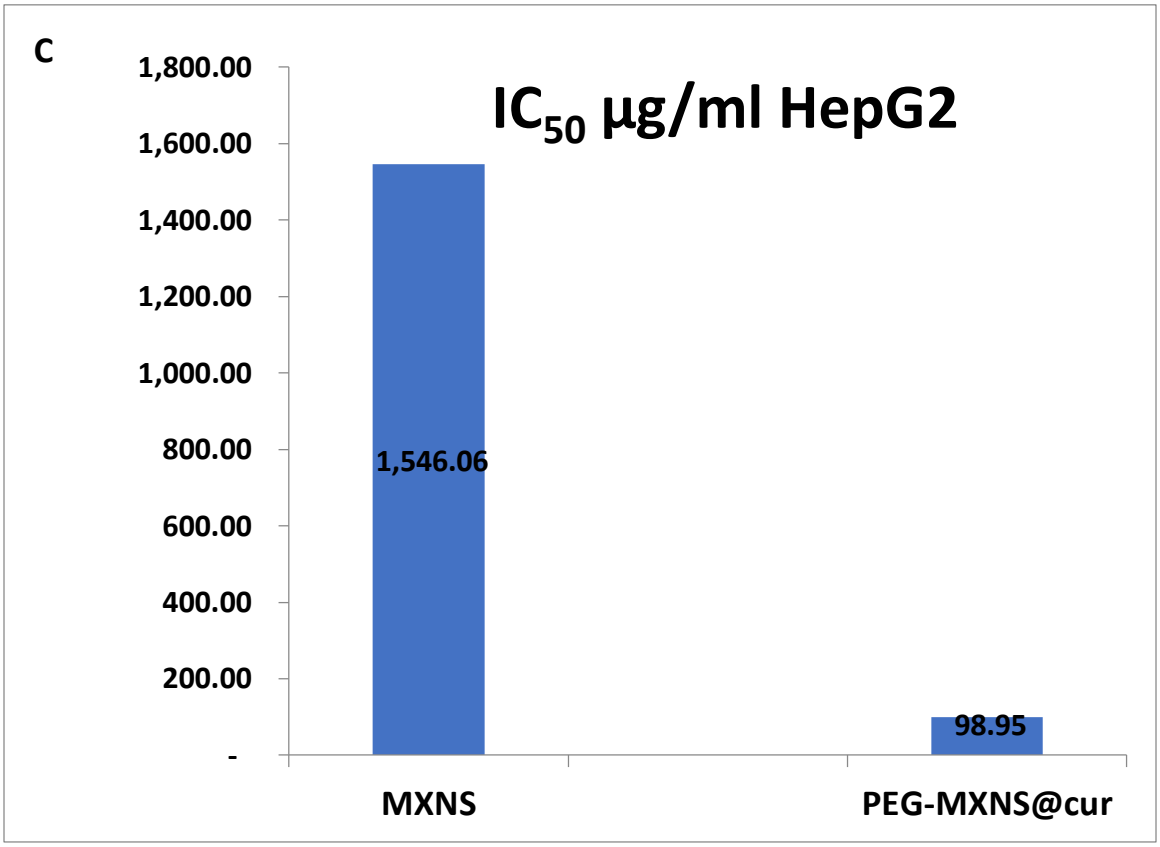

Figure 8: In-vitro study shows the effect of different concentrations of (a) MXNS, (b) PEG-MXNS@Cur on the viability of HepG2 cell line after 48 h and (c) the recorded IC_{50} of the prepared nanosheets.

Figure 9 shows the micrographs of HepG2 cells with the corresponding morphological comparison with untreated control with figure 9 (a) being the control with no change in morphology. Figure 9 (b), display the cells after 48 hours of after-treatment with various MXNS concentrations not being affected which correlate with the viability percentage previously mentioned. The number of cells decreased, and the size of the remaining cells clearly shrank after 48 hours of treating the cell lines with the various concentrations of PEG-MXNS@Cur, as shown in Figure 9 (c).

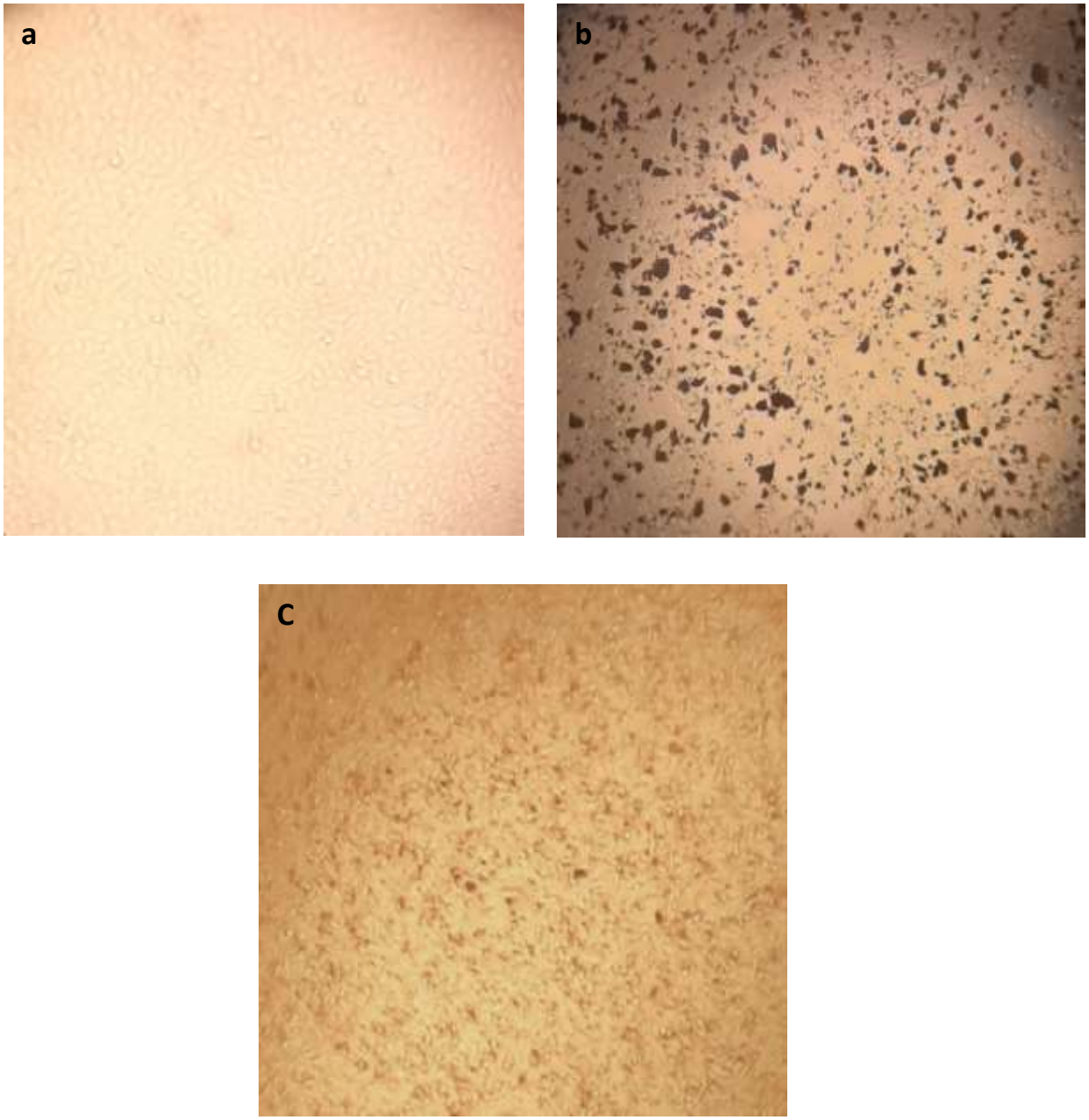
a
b
C

Figure 9: Photographs taken with an inverted microscope illustrate the modifications brought about by the as-prepared nanosheets (a) being the control for HepG2 cell line, (b) Mxene treated cells and (c) PEG-MXNS@Cur treated cancer cells.

3.6.2 Cytotoxicity measurements against MCF7

The cytotoxicity of MXNS and PEG-MXNS@Cur was determined in MCF7 cell line exposed to 0.98, 1.95, 3.91, 7.81, 15.63, 31.25, 62.5, 125, 250, 500, 1000 and 2000 µg/ml for the Mxene and to 0.98, 1.95, 3.91, 7.81, 15.63, 31.25, 62.5, 125 and 250 µg/ml for the PEG-MXNS@Cur at incubation time scale of 48 h. Analysis of cell viability revealed that prepared nanosheets dose-dependently inhibited the growth of the MCF7 cell line. Figure 10 (a) shows that Mxene caused inhibition of 20 % at a very great concentration of 2000 µg/ml which indicates that Mxene has a poor anticancer ability against MCF7 cell line with lower concentrations. Furthermore, the Mxene IC_{50} value was 886.5 µg/ml which correlates with the poor inhibition activity for the Mxene at low concentrations (figure 10 (c)). Figure 10 (b) illustrates the values for PEG-MXNS@Cur nanosheets at the peak concentration of 250 µg/ml with a viability percentage of 19.77 % which is very much lower compared to Mxene alone. These findings show that including curcumin in Mxene significantly increased its anticancer effects on breast cancer cells., which results from the DNA alteration caused by oxidative stress brought on by curcumin through the generation of ROS and oxidative damage [42]. Accordingly, the IC_{50} results of the PEG-MXNS@Cur was 90.19 µg/mL (figure 10 (c)) which is very much lower than Mxene alone indicating a better inhibition property than Mxene.

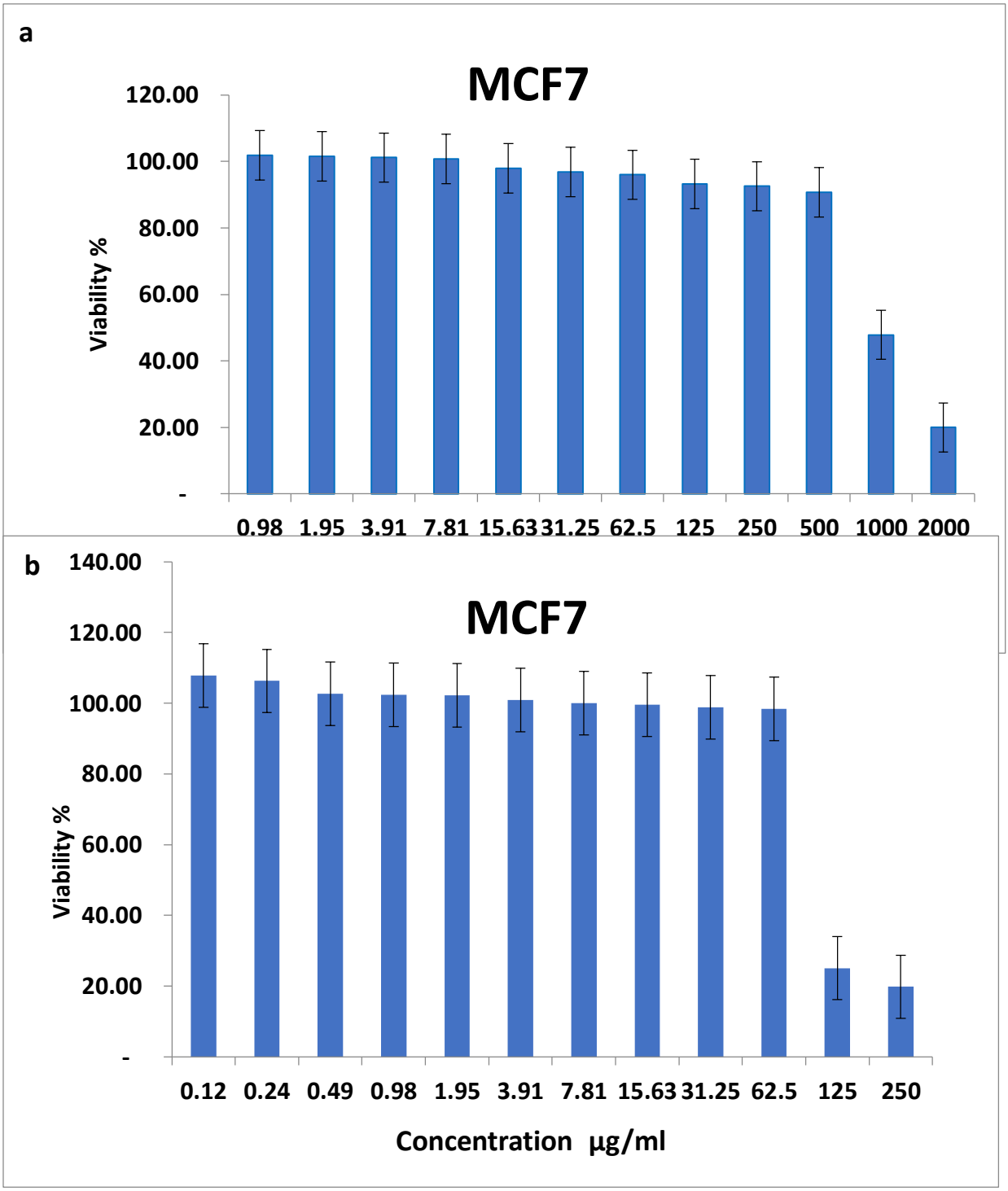
a
MCF7
120.00
100.00
80.00
60.00
40.00
20.00
-
Viability %
0.98 1.95 3.91 7.81 15.63 31.25 62.5 125 250 500 1000 2000
b
MCF7
140.00
120.00
100.00
80.00
60.00
40.00
20.00
-
Viability %
0.12 0.24 0.49 0.98 1.95 3.91 7.81 15.63 31.25 62.5 125 250
Concentration µg/ml

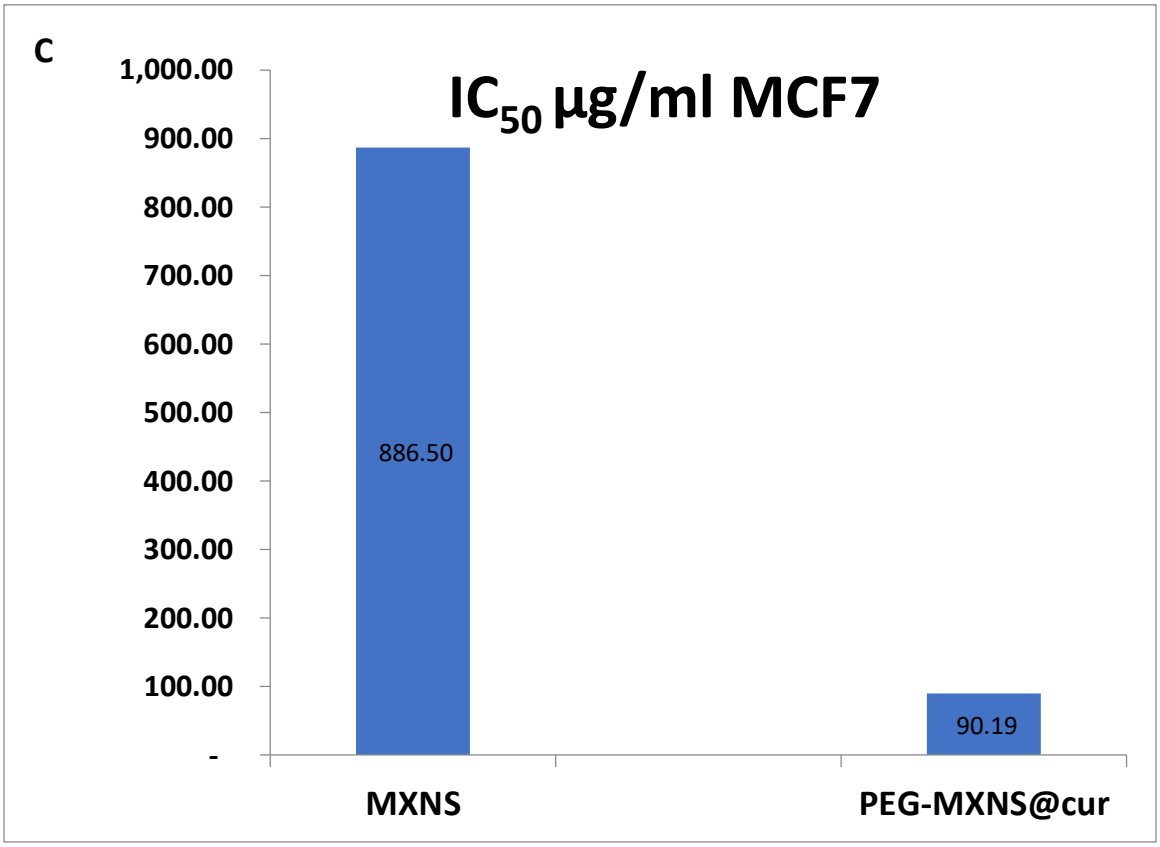

Figure 10: In-vitro study reveals the effect of various concentrations of (a) MXNS, (b) PEG-MXNS@Cur on the viability of MCF7 cell line after 48 h and (c) the recorded IC_{50} of the prepared nanosheets.

Figure 11 displays micrographs of the MCF7 cells with the matching morphological comparison with untreated control. Figure 11 (b) shows the cells after being exposed to various Mxeme doses for 48 hours are unaffected to some extent and are consistent with the previously indicated viability percentage. Figure 11 (c) the PEG-MXNS@Cur treated cells, however, show that the number of cells decreased after 48 hours of treating the cell lines with different amounts, and the surviving cells shrank noticeably with better results

on MCF7 compared to HepG2 results. Figure 11(a) shows untreated cells in the negative control group that had not undergone any morphological changes.

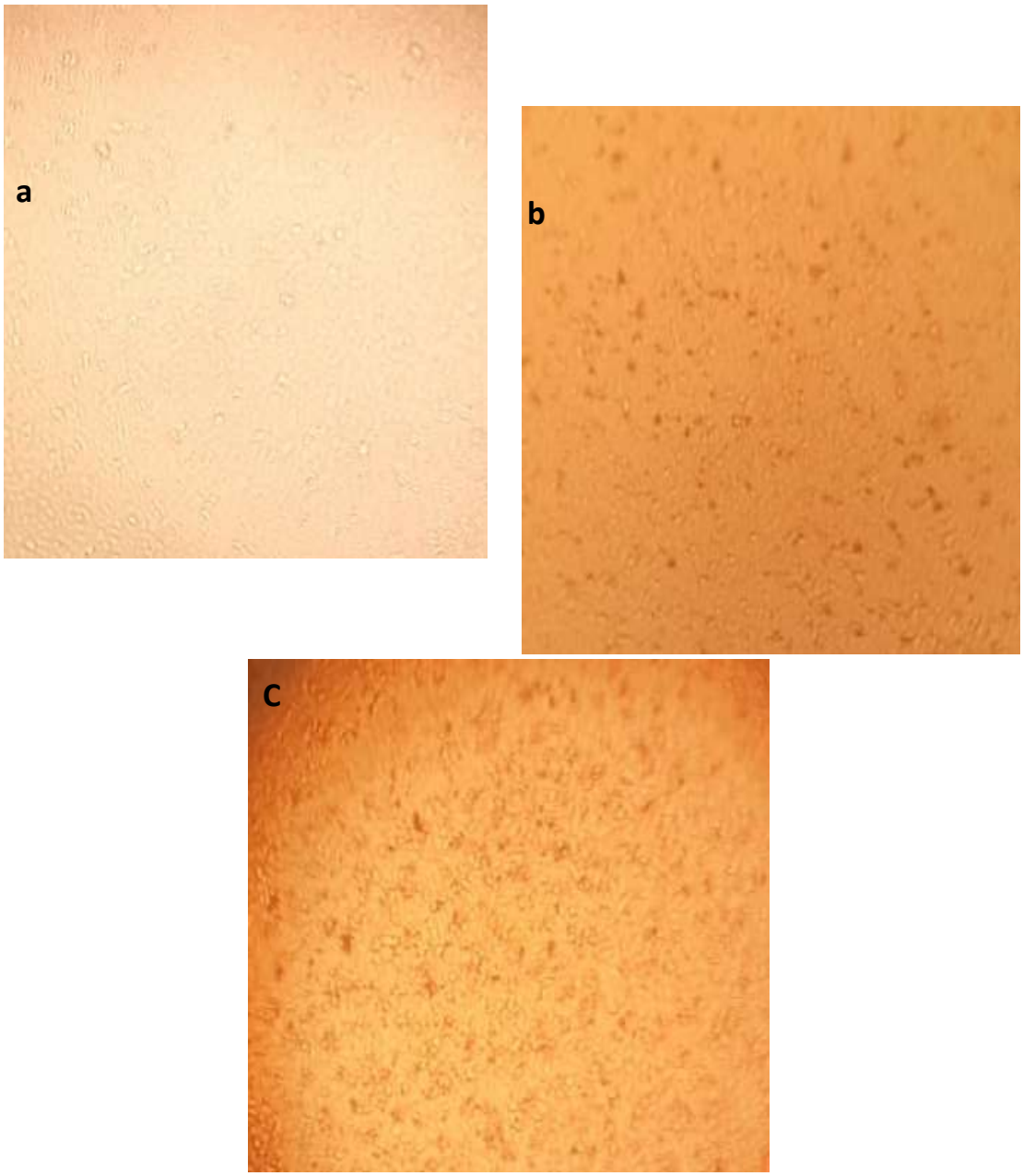

Figure 11: Inverted microscope photographs of the changes induced on the MCF7 cell lines by the prepared nanosheets with (a) being the control for the cell line, (b) Mxene treated cells, (c) PEG-MXNS@Cur treated cancer cells.

3.7 DPPH radical scavenging assay

Figure 12 (a) shows the antioxidant activity of the Mxene nanosheets of different concentrations. The DPPH free radicals were quenched in a dose-dependent manner, meaning that the inhibition increased with increasing nanosheet's concentration. Mxene showed a high scavenging percentage of 81 % for the DPPH at the peak concentration of 1000 µg/ml which is due to Mxene having an atomic scale thickness, this enables them to engage in interactions with reactive oxygen species (ROS) and even scavenge ROS at dark [43]. While at the lowermost concentration of 50 µg/ml, a percentage of less than one was shown. Furthermore, the color change outlined in figure 12 (b) proves the dose-dependent matter of the scavenging activity of the Mxene with the purple color of DPPH changing to a brighter color with increasing the concentration.

Antioxidant activities are frequently expressed in terms of inhibitory concentration (IC_{50}), or the concentration needed to achieve 50% radical scavenging [44]. The lower value of IC_{50} can be used to measure an antioxidant's efficiency [45]. When evaluating DPPH, the IC_{50} evaluates the decrease in DPPH concentration when it reaches 50% of its initial level after the addition of the antioxidant [46]. The IC_{50} value for Mxene nanosheets through this pathway was 30.7 µg/ml. This obtained IC_{50} value supports the finding that Mxene does not exhibit effective free-scavenging DPPH activity on its own compared to the addition of other components.

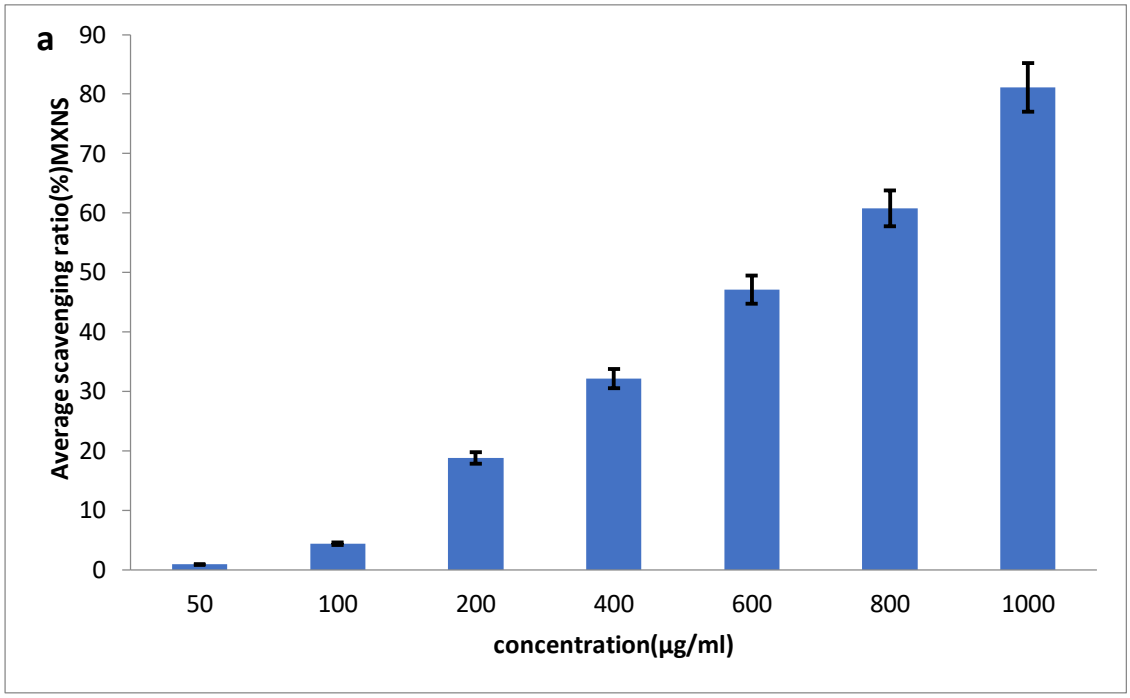

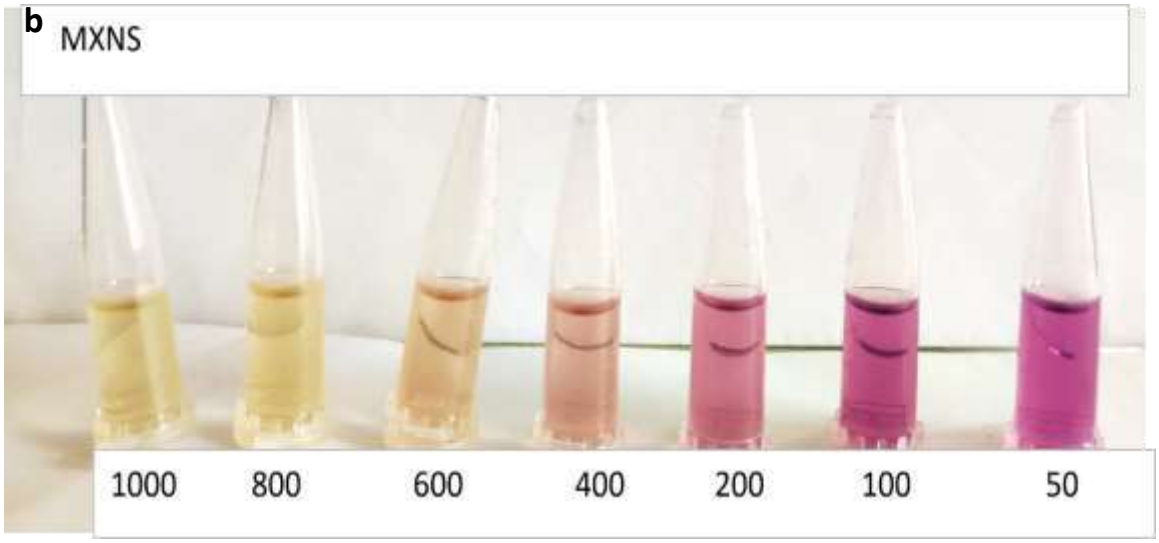

Figure 12: (a) Various concentrations of MXNS's scavenging activity (50, 100, 200, 400, 600, 800, and 1000 g/ml), (b) The color change of the DPPH solution of MXNS.

Figure 13 (a) demonstrates the scavenging activity of PEG-MXNS@cur composite at different concentrations. The antioxidant activity of the prepared nanosheets showed a higher quenching percentage of 85.6 % of the DPPH at 1000 µg/ml which is slightly higher than the Mxene alone. This is credited to the curcumin's ability to potentially scavenge the majority of ROS, a trait that causes antioxidant action in healthy cells [47]. A higher percentage of 17.5 % at the lower most concentration of 50 µg/ml was observed that was larger compared to Mxene alone. Also, an increase in the inhibition percentages of 19 and 28 % at 100 and 200 µg/ml, respectively was observed. Moreover, a very apparent color change from purple to yellow was shown in figure 13 (b) while the concentration increased, this is more obvious than Mxene alone. The IC_{50} obtained value of the PEG-MXNS@cur composite was 3.7 µg/ml, which is the lowest value of all prepared nanosheets and lower than the reported previous literature [48]. This result proves that the addition of curcumin to the Mxene has improved its efficacy of scavenging the DPPH free radical than the Mxene alone.

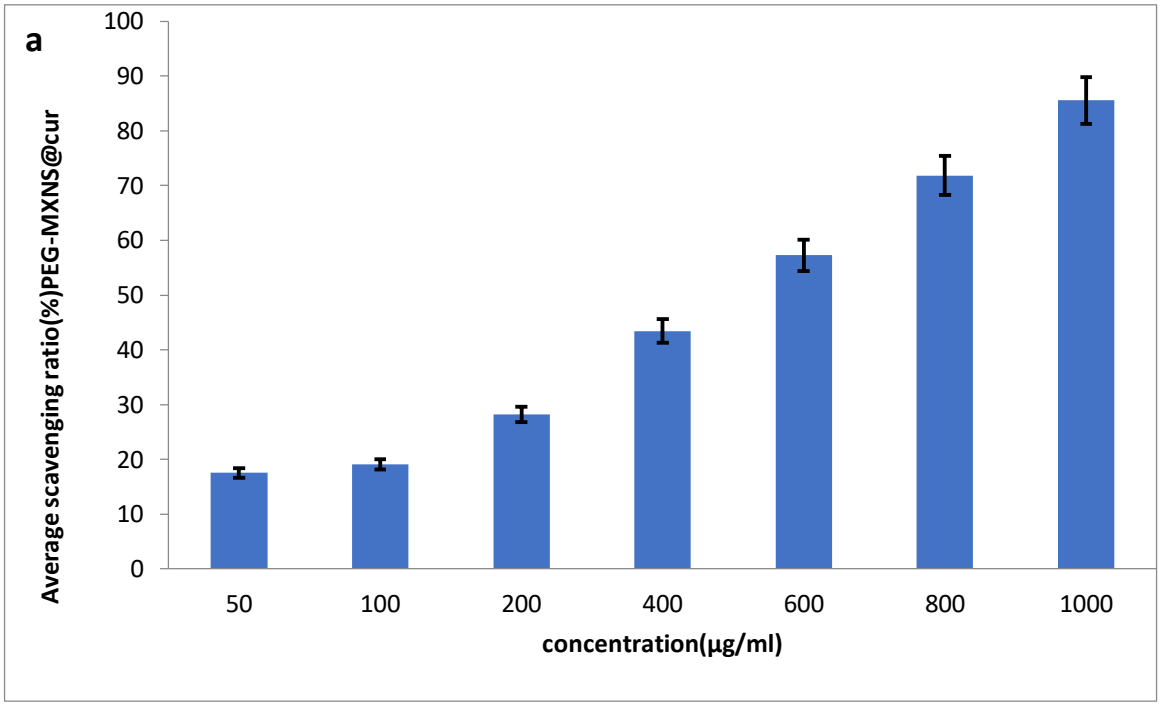
a
Average scavenging ratio(%)PEG-MXNS@cur
100
90
80
70
60
50
40
30
20
10
0
50
100
200
400
600
800
1000
concentration(µg/ml)

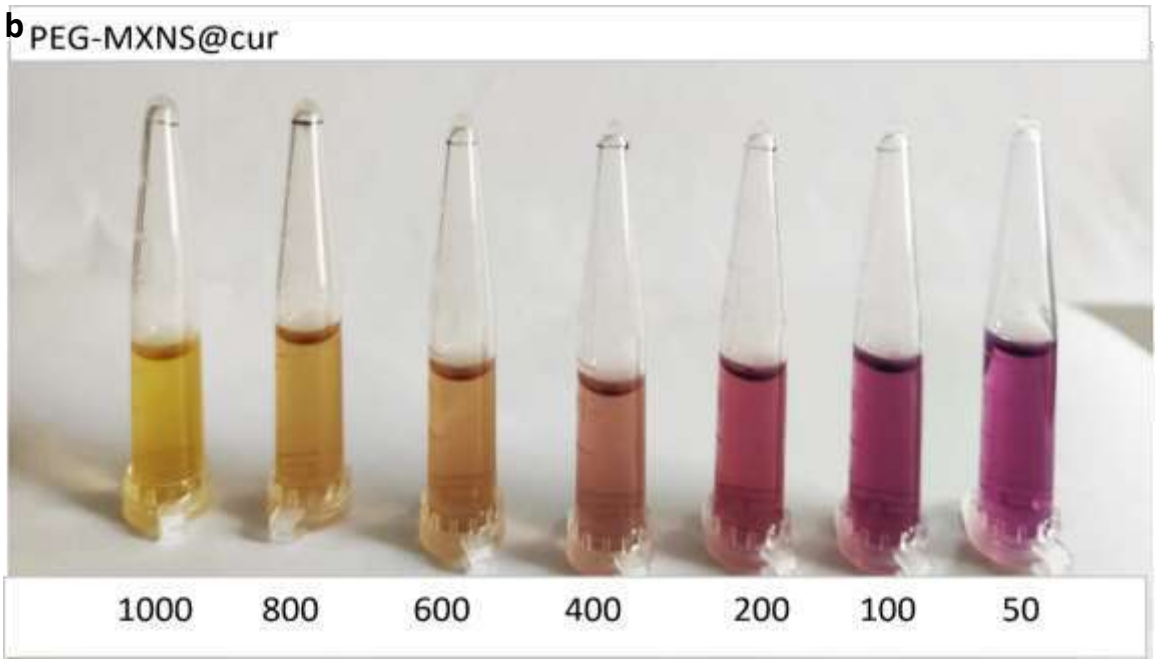
b PEG-MXNS@cur
1000
800
600
400
200
100
50

Figure 13: (a) PEG-MXNS@Cur scavenging activity at various concentrations (50, 100, 200, 400, 600, 800, and 1000 g/ml), (b) Color of the DPPH solution changed from purple to yellow of PEG-MXNS@Cur concentrations.

The antioxidant activity of the curcumin is seen in figure 14 (a) with different quantities (12.5, 25, 50, 100, 150, 200 and 250 μg/ml). Increased concentration correlates with increased suppression of DPPH free radical activity. The percentage (78%), which is slightly lower than the values for MXene alone and PEG-MXNS@cur combination, was attained at the maximum concentration of 250 g/ml, indicating that the addition of the Mxene enlarged the antioxidant activity of the curcumin. The scavenging activity of the DPPH at the lowest concentration of 12.5 μg/ml was 11.8 % which is also higher than the Mxene alone. Figure 14 (b), on the other hand, demonstrated a very noticeable color change from purple to deep yellow, demonstrating the curcumin's scavenging activity on the free radical. The IC_{50} value of the curcumin was 4.3 μg/ml which is a slightly lower value than the positive control showing a value of 8.6 μg/ml, and slightly higher than the value of the Mxene curcumin composite which gave a value of 3.7 μg/ml. This indicates that the curcumin has effective free radical scavenging activity which improved the Mxene's activity when combined with it.

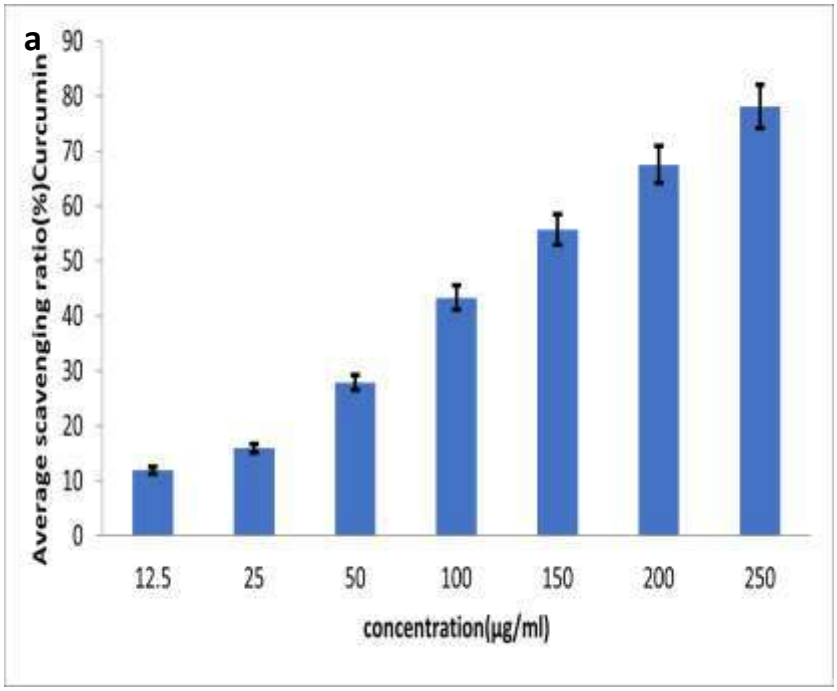
a
Average scavenging ratio(%)Curcumin
90
80
70
60
50
40
30
20
10
0
12.5
25
50
100
150
200
250
concentration(µg/ml)

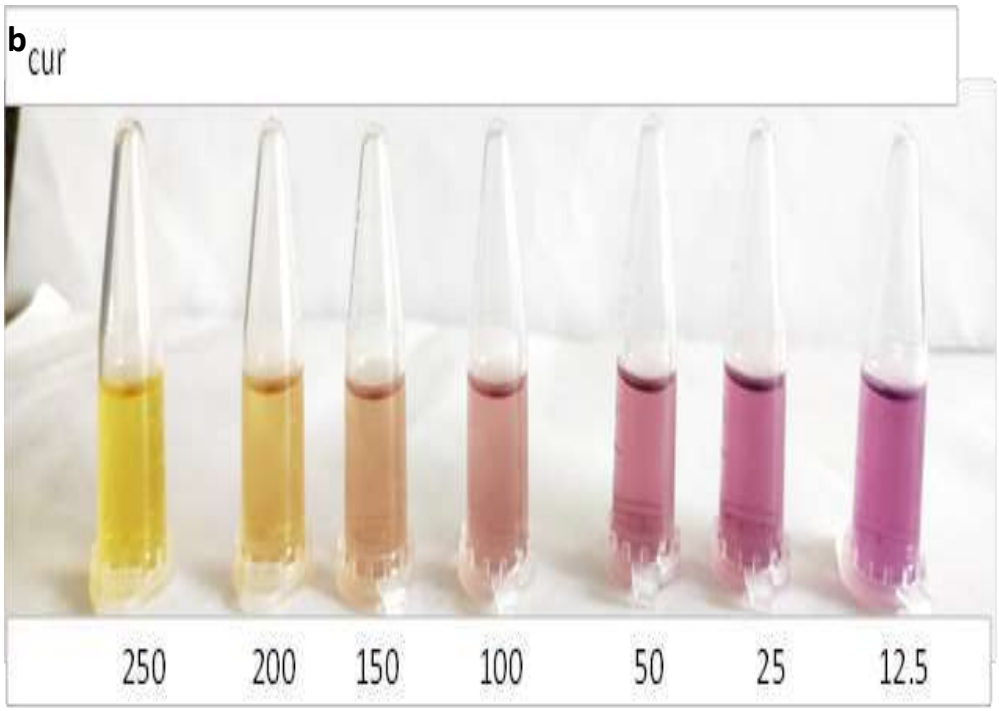
b
cur
250
200
150
100
50
25
12.5

Figure 14: (a) Scavenging activity of curcumin with diverse concentrations (12.5, 25, 50, 100, 150, 200 and 250 µg/ml), (b) With increasing curcumin concentrations, the DPPH solution's color changed from purple to a deep yellow.

The scavenging activity of the BHT which is the positive control is shown in figure 15 (a). The highest concentration of 1000 µg/ml showed an antioxidant activity percentage of only 68 % which is the lowest percentage compared to the prepared nanosheets. However, the percentage at 50 µg/ml gave a 7 % activity which is higher than the one of Mxene but lower than PEG-MXNS@cur composite and curcumin alone. This finding demonstrated how adding curcumin to Mxene increased its antioxidant properties. Also, figure 15 (b) illustrates the color change in of the DPPH with the different concentrations of the positive control BHT, showing a change from purple to a nearly yellow color at the maximum concentration. This proves that the prepared nanosheets have a better activity than the standard. The IC_{50} value for BHT was 8.6 µg/ml that is lower than the reported numbers in the previous literature [49, 47]. This obtained IC_{50} value supports the finding that Mxene curcumin shows a better effective free-scavenging DPPH activity compared to the positive control.

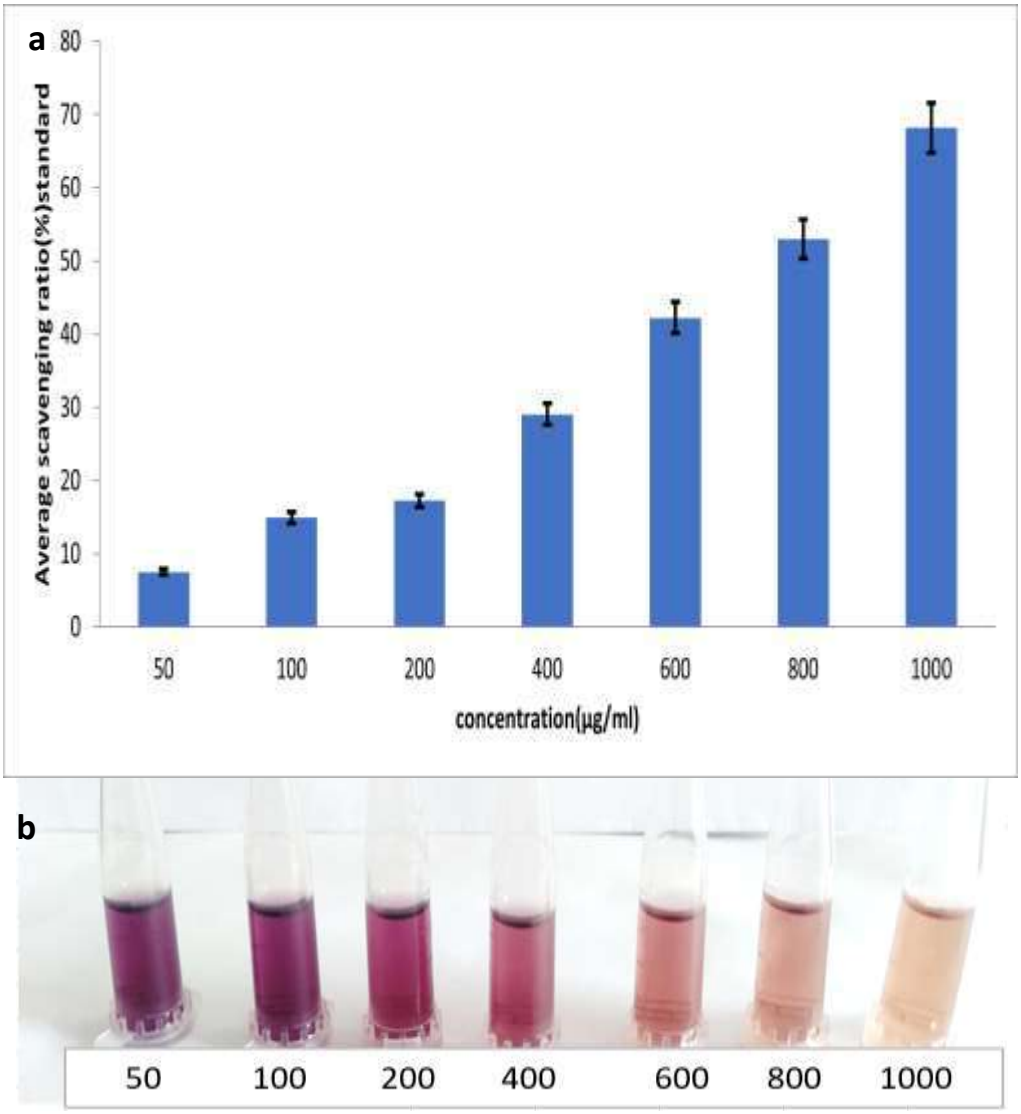

Figure 15: (a) Scavenging activity of standard BHT with diverse concentrations (50, 100, 200, 400, 600, 800 and 1000 µg/ml), (b): Color of the DPPH solution changed from purple to yellow of standard concentrations.

3.8 Drug release profile

To evaluate the efficiency of nanosheet-based drug delivery systems, an in vitro release profile was studied. The efficacy of curcumin depends on how it releases from its nanosheet-based delivery mechanism in a simulated tumor microenvironment. This is why when the nanosheets were exposed to a lower pH setting, curcumin release was observed. Curcumin loaded Mxene nanosheets were evaluated for controlled drug release in pH 5.5, 7.4. As shown in figure 16, at pH 5.5 the PEG-MXNS@cur showed quick release with a cumulative release 53% at 24 h and 73.5% at 96 h. The release of curcumin from Mxene nanosheets was observed to be at a quicker rate, followed by a prolonged and sustain release. While at pH 7.4, curcumin was released slowly only about 1.4 % at 24 h and 2.25% at 96 h. Mxene nanosheets containing curcumin could achieve effective, long-term, and controlled pH-stimulated release of curcumin. The designed 2D pH responsive as a drug delivery system, Mxene not only keeps curcumin from degrading but also sustains its release.

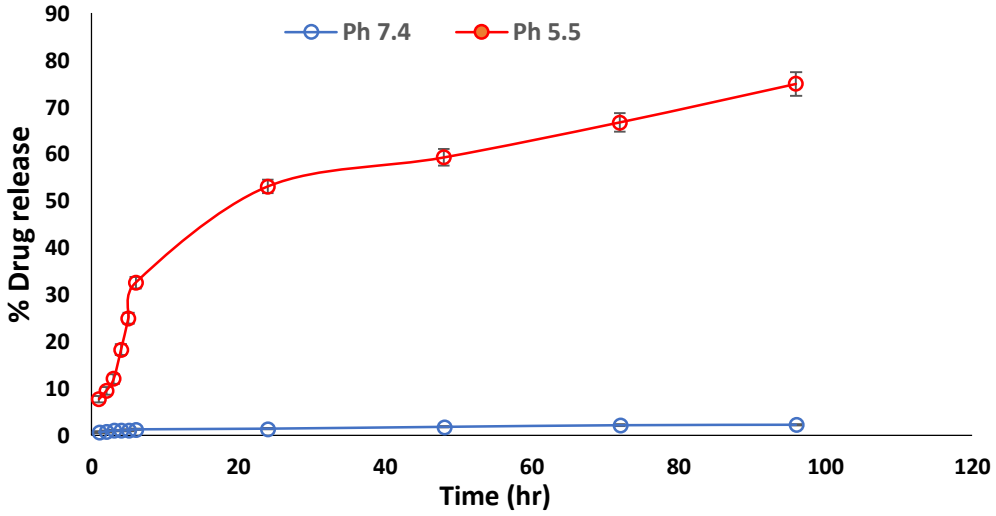

Figure 16: Curcumin release from PEG-MX@cur at pH 7.4 and pH 5.5 at various intervals of time.

3.9 Encapsulation efficiency measurements

An important metric for evaluating a delivery system's loading capacity is encapsulation ability. To determine the biological activity of curcumin, the overall amount of curcumin encapsulation in PEG-MXNS@cur was evaluated. High encapsulation efficiency was demonstrated by the synthesised PEG-MXNS@cur, which reached 99 ± 0.011%. PEG-MXNS@cur calculated curcumin encapsulation efficiency outperformed that of earlier research, indicating that it is a reliable means of delivering curcumin [50].

4. Conclusion

1. Modified Ultrathin-MXene was successfully synthesized and characterized for biomedical applications using a facile selective etching process.
2. The Modified Ultrathin-MXene was loaded with Curcumin to study its biocompatibility.
3. The Mxene loaded Curcumin exhibited good UV shielding and acceptance of Curcumin in the Mxene solution supported by the zeta potential values.

References

1. Bray F, Ferlay J, Soerjomataram I, Siegel RL, Torre LA, Jemal A. Global cancer statistics 2018: GLOBOCAN estimates of incidence and mortality worldwide for 36 cancers in 185 countries. CA Cancer J Clin. 2018;68(6):394-424.
2. Thoidingjam S, Tiku AB. New developments in breast cancer therapy: role of iron oxide nanoparticles. Advances in Natural Sciences: Nanoscience and Nanotechnology. 2017;8(2):023002

3. Darwesh, R., & Elbialy, N. S. (2021). Iron oxide nanoparticles conjugated curcumin to promote high therapeutic efficacy of curcumin against hepatocellular carcinoma. Inorganic Chemistry Communications, 126, 108482.
4. N. Amanlou, M. Parsa, K. Rostamizadeh, S. Sadighian, F. Moghaddam, Enhanced cytotoxic activity of curcumin on cancer cell lines by incorporating into gold/ chitosan nanogels, Mater. Chem. Phys. 226 (2019) 151–157.
5. Naguib, M.; Kurtoglu, M.; Presser, V.; Lu, J.; Niu, J.; Heon, M.; Hultman, L.; Gogotsi, Y.; Barsoum, M.W. (2011). "Two-Dimensional Nanocrystals Produced by Exfoliation of Ti3AlC2". Advanced Materials. 23 (37): 4248–4253.
6. Naguib, M.; Mochalin, V.N.; Barsoum, M.W.; Gogotsi, Y. (2011). "25th Anniversary Article: MXenes: A New Family of Two-Dimensional Materials". Advanced Materials. 26 (7): 992–1005
7. Huang, J., Li, Z., Mao, Y., & Li, Z. (2021). Progress and biomedical applications of MXenes. *Nano Select*, *2*(8), 1480-1508.
8. Lin, H.; Wang, X.; Yu, L.; Chen, Y.; Shi, J. Two-Dimensional Ultrathin MXene Ceramic Nanosheets for Photothermal Conversion. Nano Lett. 2017, 17, 384–391.
9. Kizhakkayil J, Thayyullathil F, Chathoth S, Hago A, Patel M, Galadari S. Modulation of curcumin-induced Akt phosphorylation and apoptosis by PI3K inhibitor in MCF-7 cells. *Biochem Biophys Res Commun.* 2010;**394**(3):476–81.
10. Lv ZD, Liu XP, Zhao WJ, Dong Q, Li FN, Wang HB, et al. Curcumin induces apoptosis in breast cancer cells and inhibits tumor growth in vitro and in vivo. Int J Clin Exp Pathol. 2014;7(6):2818–24.
11. Chen CC, Sureshbabul M, Chen HW, Lin YS, Lee JY, Hong QS, et al. Curcumin Suppresses Metastasis via Sp-1, FAK Inhibition, and E-Cadherin Upregulation in Colorectal Cancer. Evid Based Complement Alternat Med. 2013;2013:541695.
12. W. Chen, J. Ouyang, X. Yi, Y. Xu, C. Niu, W. Zhang, L. Wang, J. Sheng, L. Deng, Y. N. Liu and S. Guo, Adv. Mater., 2018, 30, 1703458–1703464.
13. X. Ren, M. Huo, M. Wang, H. Lin, X. Zhang, J. Yin, Y. Chen and H. Chen, ACS Nano, 2019, 13, 6438–6454.

14. Z. Wang, K. Yi, Q. Lin, L. Yang, X. Chen, H. Chen, Y. Liu and D. Wei, Nat. Commun., 2019, 10, 1544–1553.
15. C. Zheng, X. Jin, Y. Li, J. Mei, Y. Sun, M. Xiao, H. Zhang, Z. Zhang and G. J. Zhang, Sci. Rep., 2019, 9, 759–767.
16. Zamhuri, A.; Lim, G. P.; Ma, N. L.; Tee, K. S.; Soon, C. F. J. B. e. o. MXene in the lens of biomedical engineering: synthesis, applications, and outlook. Biomedical engineering online 2021, 20, 33, DOI: 10.1186/s12938-021-00873-9.
17. Philoppes, J. N., & Lamie, P. F. (2019). Design and synthesis of new benzoxazole/benzothiazole-phthalimide hybrids as antitumor-apoptotic agents. Bioorganic chemistry, 89, 102978.
18. J.M. Edmondson, L.S.Armstrong, A.O. Martinez, Manual of microbiologic monitoring of laboratory animals,J. Tiss. Cult.Meth.11(1988), 5.
19. Ahmed, E. A., Mohamed, M. F., Omran, A., & Salah, H. (2020). Synthesis, EGFR-TK inhibition and anticancer activity of new quinoxaline derivatives. Synthetic Communications, 50(19), 2924-2940.
20. Chen, L.; Zhang, Y.; Liu, J.; Wang, W.; Li, X.; Zhao, L.; Wang, W.; Li, B. Novel 4-Arylaminoquinazoline Derivatives with (E)-Propen-1-yl Moiety as Potent EGFR Inhibitors with Enhanced Antiproliferative Activities against Tumor Cells. Eur. J. Med. Chem. 2017, 138, 689–697.
21. Dai, F.; Li, Q.; Wang, Y.; Ge, C.; Feng, C.; Xie, S.; He, H.; Xu, X.; Wang, C. Design, Synthesis, and Biological Evaluation of Mitochondria-Targeted Flavone-Naphthalimide- Polyamine Conjugates with Antimetastatic Activity. J. Med. Chem. 2017, 60, 2071–2083.
22. Tang, Q.; Zhao, Y.; Du, X.; Chong, L.; Gong, P.; Guo, C. Design, Synthesis, and Structure- Activity Relationships of Novel 6,7-Disubstituted-4-Phenoxyquinoline Derivatives as Potential Antitumor Agents. Eur. J. Med. Chem. 2013, 69, 77–89.
23. Youssif, B. G. M.; Abdelrahman, M. H.; Abdelazeem, A. H.; Abdelgawad, M. A.; Ibrahim, H. M.; Salem, O. I. A.; Mohamed, M. F. A.; Treambleau, L.; Nasir, S.;

Bukhari, A. Design, Synthesis, Mechanistic and Histopathological Studies of Small-Molecules of Novel Indole- 2-Carboxamides and Pyrazino [1,2-a]Indol-1(2H)-Ones as Potential Anticancer Agents Effecting the Reactive Oxygen Species Production. Eur. J. Med. Chem. 2018, 146, 260–273.

24. A. Sudha, J. Jayachandran, P. Srinivasan, Green synthesis of silver nanoparticles using Lippianodiflora aerial extract and evaluation of their antioxidant.
25. Teixeira, P. V., Adega, F., Martins-Lopes, P., Machado, R., Lopes, C. M., & Lúcio, M. (2023). pH-Responsive Hybrid Nanoassemblies for Cancer Treatment: Formulation Development, Optimization, and In Vitro Therapeutic Performance. Pharmaceutics, 15(2), 326.
26. Yunfei Huang, Yiling Zhan, Guangyi Luo, Yan Zeng, David Julian McClements, Kun Hu, Curcumin encapsulated zein/caseinate-alginate nanoparticles: Release and antioxidant activity under in vitro simulated gastrointestinal digestion, Current Research in Food Science, Volume 6, 2023, 100463, ISSN 2665-9271, https://doi.org/10.1016/j.crfs.2023.100463.
27. Satheeshkumar, E., Makaryan, T., Melikyan, A. et al. One-step Solution Processing of Ag, Au and Pd@MXene Hybrids for SERS. Sci Rep 6, 32049 (2016).
28. Q. Xue, H. Zhang, M. Zhu, Z. Pei, H. Li, Z. Wang, Y. Huang, Y. Huang, Q. Deng, J. Zhou, S. Du, Q. Huang and C. Zhi, Adv., Mater., 2017, 29, 1604847.
29. Dai, F.; Li, Q.; Wang, Y.; Ge, C.; Feng, C.; Xie, S.; He, H.; Xu, X.; Wang, C. Design, Synthesis, and Biological Evaluation of Mitochondria-Targeted Flavone-Naphthalimide- Polyamine Conjugates with Antimetastatic Activity. J. Med. Chem. 2017, 60, 2071–2083.
30. Xie, Y.; Rahman, M.M.; Kareem, S.; Dong, H.; Qiao, F.; Xiong, W.; Liu, X.; Li, N.; Zhao, X. Facile synthesis of CuS/MXene nanocomposites for efficient photocatalytic hydrogen generation. CrystEngComm 2020, 22, 2060–2066.

31. Tang, R.; Zhou, S.; Li, C.; Chen, R.; Zhang, L.; Zhang, Z.; Yin, L. Janus-Structured Co-Ti3C2 MXene Quantum Dots as a Schottky Catalyst for High-Performance Photoelectrochemical Water Oxidation. Adv. Funct. Mater. 2020, 30, 2000637.
32. Luo, Q.; Chai, B.; Xu, M.; Cai, Q. Preparation, and photocatalytic activity of TiO2-loaded Ti3C2 with small interlayer spacing. Appl. Phys. A 2018, 124, 495. [CrossRef]
33. Xuan, J.; Wang, Z.; Chen, Y.; Liang, D.; Cheng, L.; Yang, X.; Liu, Z.; Ma, R.; Sasaki, T.; Geng, T. Organic-base-driven intercalation and delamination to produce functionalized titanium carbide nanosheets with superior photothermal therapeutic performance. Angew. Chem. 2016, 128, 14789–14794. [CrossRef].
34. Subhan, M. A., Alam, K., Rahaman, M. S., Rahman, M. A., & Awal, R. (2013). Synthesis and Characterization of Metal Complexes Containing Curcumin (C₂₁H₂₀O₆) and Study of their Anti-microbial Activities and DNA-binding Properties. Journal of Scientific Research,2014, 6(1), 97–109.
35. A. M. Jastrzębska, E. Karwowska, P. Kurtycz, A. R. Olszyna, A. Kunicki, Surf. Coat. Technol.2015. 271.
36. A. M. Jastrzębska, J. Jureczko, A. R. Kunicki, A. R. Olszyna, Int. J. Appl. Ceram. Technol. 2015. 12.
37. A. M. Jastrzębska, J. Jureczko, A. R. Kunicki, A. R. Olszyna, Int. J. Appl. Ceram. Technol. 2015. 12.
38. Kang, R., Zhang, Z., Guo, L. et al. Enhanced Thermal Conductivity of Epoxy Composites Filled with 2D Transition Metal Carbides (MXenes) with Ultralow Loading. Sci Rep 9, 9135 (2019).
39. Naguib M, Kurtoglu M, Presser V, Lu J, Niu J, Heon M, Hultman L, Gogotsi Y, Barsoum MW. Two-dimensional nanocrystals produced by exfoliation of Ti3 AlC2. Adv Mater. 2011 Oct 4;23(37):4248-53.

40. Naguib M, Kurtoglu M, Presser V, Lu J, Niu J, Heon M, Hultman L, Gogotsi Y, Barsoum MW. Two-dimensional nanocrystals produced by exfoliation of Ti3 AlC2. Adv Mater. 2011 Oct 4;23(37):4248-53.
41. Zhang J, Li S, Hu S, Zhou Y. Chemical Stability of Ti_3C_2 MXene with Al in the Temperature Range 500-700 °C. Materials (Basel). 2018 Oct 15;11(10):1979.
42. Kumar, R., Maji, B. C., & Krishnan, M. (2020). Synthesis of 2D material MXene from Ti3AlC2 MAX-phase for electromagnetic shielding applications. DAE SOLID STATE PHYSICS SYMPOSIUM 2019.
43. Ruiyang Kang, Zhenyu Zhang, Liangchao Guo, Junfeng Cui, Yapeng Chen, Xiao Hou, Bo Wang, Cheng-Te Lin, Nan Jiang & Jinhong Yu; Enhanced Thermal Conductivity of Epoxy Composites Filled with 2D Transition Metal Carbides (MXenes) with Ultralow Loading. Sci Rep 9, 9135 (2019).
44. Qu, K., Huang, K. & Xu, Z. Recent progress in the design and fabrication of MXene-based membranes. Front. Chem. Sci. Eng. 15, 820–836 (2021).
45. Yu T, Dohl J, Elenberg F, Chen Y and Deuster P: Curcumin induces concentration-dependent alterations in mitochondrial function through ros in c2c12 mouse myoblasts. J Cell Physiol 234(5): 6371- 6381, 2019. PMID: 30246249.
46. Darwesh, R., & Elbialy, N. S. (2021). Iron oxide nanoparticles conjugated curcumin to promote high therapeutic efficacy of curcumin against hepatocellular carcinoma. Inorganic Chemistry Communications, 126, 108482.
47. Chen CC, Sureshbabul M, Chen HW, Lin YS, Lee JY, Hong QS, et al. Curcumin Suppresses Metastasis via Sp-1, FAK Inhibition, and E-Cadherin Upregulation in Colorectal Cancer. Evid Based Complement Alternat Med. 2013; 2013:541695.
48. Wang, L., Li, Y., Zhao, L., Qi, Z., Gou, J., Zhang, S., & Zhang, J. Z. (2020). Recent advances in ultrathin two-dimensional materials and biomedical applications for reactive oxygen species generation and scavenging. Nanoscale, 12(38), 19516-19535.

49. Chen, Z.; Bertin, R.; Froldi, G. EC50 estimation of antioxidant activity in DPPH* assay using several statistical programs. Food Chem. 2013, 138, 414–420.
50. Sari, T. P., Mann, B., Kumar, R., Singh, R. R. B., Sharma, R., Bhardwaj, M., & Athira, S. (2015). Preparation and characterization of nanoemulsion encapsulating curcumin. *Food Hydrocolloids*, *43*, 540-546.